

SCIENCE OF TSUNAMI HAZARDS

Journal of Tsunami Society International

Volume 35

Number 1

2016

DETECTION OF TSUNAMI RADIATION AT ILLAPEL, CHILE ON 2015-9-16

BY REMOTE SENSING

1

Frank C Lin^{1,*}, Kingkarn Sookhanaphibarn¹, Worawat Choensawat¹,

**¹Multimedia Intelligent Technology Laboratory, School of Science and
Technology, Bangkok University, Rama 4 Rd, Khlong Toei, Bangkok 10110,
THAILAND**

**George Pararas-Carayannis - Tsunami Society International, Honolulu,
Hawaii 96815, USA**

**THE ECONOMIC EVALUATION AND POTENTIAL SIGNIFICANCE OF AN
EARLY RELOCATION VERSUS COMPLETE DESTRUCTION BY A POTENTIAL
TSUNAMI OF A COASTAL CITY IN ECUADOR**

18

**Fabian Rodriguez, Mario Cruz D'Howitt, Theofilos Toulkeridis, Rodolfo Salazar,
Gioconda Elizabeth Ramos Romero, Veleria Alejandra Recalde Moya and
Oswaldo Padilla**

Universidad de las Fuerzas Armadas ESPE, Sangolquí, ECUADOR

TSUNAMI SOCIETY INTERNATIONAL, 1741 Ala Moana Blvd. #70, Honolulu, HI 96815, USA.

SCIENCE OF TSUNAMI HAZARDS is a CERTIFIED OPEN ACCESS Journal included in the prestigious international academic journal database DOAJ, maintained by the University of Lund in Sweden with the support of the European Union. SCIENCE OF TSUNAMI HAZARDS is also preserved, archived and disseminated by the National Library, The Hague, NETHERLANDS, the Library of Congress, Washington D.C., USA, the Electronic Library of Los Alamos, National Laboratory, New Mexico, USA, the EBSCO Publishing databases and ELSEVIER Publishing in Amsterdam. The vast dissemination gives the journal additional global exposure and readership in 90% of the academic institutions worldwide, including nation-wide access to databases in more than 70 countries.

OBJECTIVE: Tsunami Society International publishes this interdisciplinary journal to increase and disseminate knowledge about tsunamis and their hazards.

DISCLAIMER: Although the articles in SCIENCE OF TSUNAMI HAZARDS have been technically reviewed by peers, Tsunami Society International is not responsible for the veracity of any statement, opinion or consequences.

EDITORIAL STAFF

Dr. George Pararas-Carayannis, Editor
<mailto:drgeorgepc@yahoo.com>

EDITORIAL BOARD

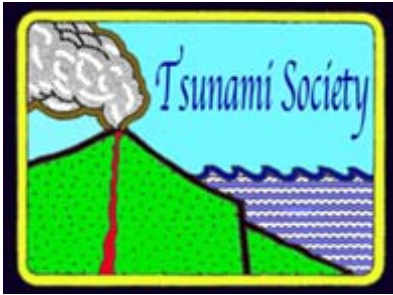
Dr. Charles MADER, Mader Consulting Co., Colorado, New Mexico, Hawaii, USA
Dr. Hermann FRITZ, Georgia Institute of Technology, USA
Prof. George CURTIS, University of Hawaii -Hilo, USA
Dr. Tad S. MURTY, University of Ottawa, CANADA
Dr. Zygmunt KOWALIK, University of Alaska, USA
Dr. Galen GISLER, NORWAY
Prof. Kam Tim CHAU, Hong Kong Polytechnic University, HONG KONG
Dr. Jochen BUNDSCHUH, (ICE) COSTA RICA, Royal Institute of Technology, SWEDEN
Dr. Yurii SHOKIN, Novosibirsk, RUSSIAN FEDERATION
Dr. Radianta Triatmadja - Tsunami Research Group, Universitas Gadjah Mada, Yogyakarta, INDONESIA

TSUNAMI SOCIETY INTERNATIONAL, OFFICERS

Dr. George Pararas-Carayannis, President;
Dr. Tad Murty, Vice President;
Dr. Carolyn Forbes, Secretary/Treasurer.

Submit manuscripts of research papers, notes or letters to the Editor. If a research paper is accepted for publication the author(s) must submit a scan-ready manuscript, a Doc, TeX or a PDF file in the journal format. Issues of the journal are published electronically in PDF format. There is a minimal publication fee for authors who are members of Tsunami Society International for three years and slightly higher for non-members. Tsunami Society International members are notified by e-mail when a new issue is available. Permission to use figures, tables and brief excerpts from this journal in scientific and educational works is granted provided that the source is acknowledged.

Recent and all past journal issues are available at: <http://www.TsunamiSociety.org> CD-ROMs of past volumes may be purchased by contacting Tsunami Society International at postmaster@tsunamisociety.org Issues of the journal from 1982 thru 2005 are also available in PDF format at the U.S. Los Alamos National Laboratory Library <http://epubs.lanl.gov/tsunami/>

**DETECTION OF TSUNAMI RADIATION AT ILLAPEL, CHILE ON 2015-9-16 BY
REMOTE SENSING****Frank C Lin^{1,*}, Kingkarn Sookhanaphibarn¹, Worawat Choensawat¹,
George Pararas-Carayannis²**¹Multimedia Intelligent Technology Laboratory, School of Science and
Technology, Bangkok University, Rama 4 Rd, Khlong Toei, Bangkok
10110, Thailand²Tsunami Society International, Honolulu, Hawaii 96815, USA**ABSTRACT**

We have detected the Tsunami Radiation generated by the 8.3 magnitude seaquake at Illapel, Chile on 2015-9-16 at the following wavelengths: 3.9 μm , 6.5 μm , 10.7 μm , and 13.3 μm . No radiation is detected at 0.63 μm , which is in the visible spectrum. The Tsunami Signals that we have observed did not decay within 44 minutes. From the satellite the Peru-Chilean Trench is visible in infrared space. In order to facilitate research in this field we attach the MATLAB code in an Appendix.

Keywords: *Tsunami Radiation, Tsunami Signal, Remote Sensing, Tsunami Decay, Illapel Chile*

*Corresponding author. Email: linbfrank@gmail.com. Tel/Fax: +662 612 4705

1. INTRODUCTION

As reported by the USGS and others [USGS, 2015], on 16 September 2015 an earthquake with epicenter at 31.577° S, and 71.652 W., occurred at 19:54:33, Chile Standard Time (22:54:33 UTC), 46 km offshore from Illapel, Chile. Based on analysis of the moment tensor, the USGS determined that the nodal plane of this event had a strike of 4.0 deg., a dip of 19.0 deg., and that the seismic moment release was 3.2×10^{28} dyn-cm, corresponding to Moment Magnitude of $M_w = 8.3$. The initial quake lasted three minutes and was followed by several aftershocks greater than magnitude six. The Chilean government reported 13 deaths and 6 persons missing. The relatively minor damage and small loss of life caused by a quake of this magnitude and of the tsunami it generated, was largely due to low population density in the region and to the unique bathymetry and coastal geomorphology along this segment of the Chilean coastline.

The earthquake was caused by thrust faulting on the interface between the Nazca and the South American tectonic plates in Central Chile. As it has been postulated for Peru and Chile, the angle of subduction of the Nazca oceanic plate beneath South America is not uniform along the entire segment of the Peru-Chile Trench. Furthermore, the relatively narrow zone of subduction is affected by buoyancy forces of the bounding oceanic ridges and fractures and is characterized by shallow earthquakes that can generate destructive tsunamis of varied intensities (Pararas-Carayannis, 2012). Specifically at the latitude of this particular event, the Nazca plate is moving towards the east-northeast at a velocity of 74 mm/yr with respect to South America and begins subducting beneath the continent, 85 km to the west of the area which was affected by the 16 September 2015 earthquake. The size, location, depth and mechanism of this event in central Chile, are all consistent with its occurrence on the megathrust interface in this region. The anomalous, rupturing in opposing directions probably had a diminishing effect on tsunami generating efficiency.

As it was indicated for the 2011 Japan earthquake (Pararas-Carayannis, 2014), unusual clustering and chronological sequencing of aftershocks are indicative of segmented and gradual release of tectonic stress. For the event in Chile, the energy was also released gradually by separate events on adjacent faults and this may partially account for observations of different degrees of inundation along the Bay of Valparaiso and of the tsunami's directional approach as well as for the lesser, far-field tsunami impact (Pararas-Carayannis, report in prep.)

The area affected by the earthquake is estimated to have been about 230x100 km, or more concisely 23,000 sq. km. By comparison, the distance from Illapel to Santiago is approximately 230 km. The vastness of the quake-affected area had a bearing on the decay rate of the tsunami radiation signal, as we shall demonstrate. Preliminary evaluation of the source mechanism of tsunami generation associated with this earthquake - as inferred from geologic structure, rupturing process, seismic intensities, spatial distribution of aftershocks, energy release and fault plane solutions - indicates that heterogeneous crustal displacements took place along the entire length of the earthquake rupture (Pararas-Carayannis, report in prep.)

The tsunami impacted the entire Pacific region. Locally, preliminary post-disaster surveys in the vicinity of Valparaiso Bay, showed that the tsunami had a focused impact along certain locations in the Coquimbo coastal area, where maximum runup of up to 6 meters caused significant damage. Other impacted villages were Concon, Los Vilos and Tongoy, where the tsunami runup varied considerably ranging from less than 2 meters and up to 3-5 meters in certain locations. As reported by the USGS, the tsunami was recorded with the following maximum wave amplitudes in meters at these selected tide stations: 4.75 at Coquimbo, 1.78 at Valparaiso, 0.88 at Constitucion, 0.83 on Easter Island, 0.67 at Pago Pago, American Samoa; 0.15 at Quepos, Costa Rica; 0.56 on Isla Santa Cruz, Ecuador; 1.37 on NukuHiva, French Polynesia; 0.26 at Kushimoto, Japan; 0.37 at Puerto Angel, Mexico; 0.35 on Chatham Islands, New Zealand; 0.55 at La Punta, Peru; 0.44 at Shikotan, Russia; 0.34 at Ventura, California; and 0.90 at Hilo, Hawaii.

The map below shows the directivity of tectonic plate movements along the boundaries of the Nazca plate [Wikipedia, 2015].

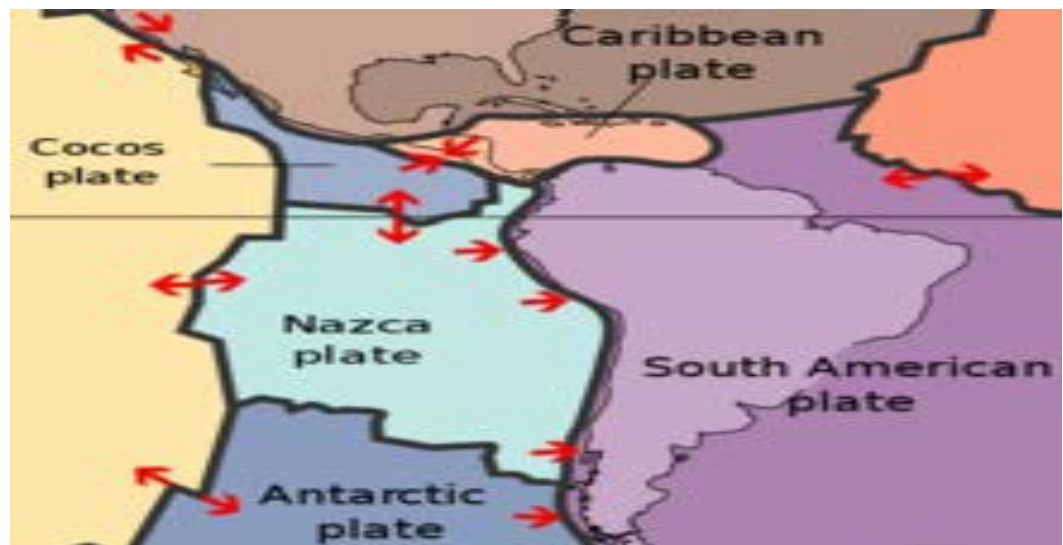


Fig.1: Tectonic motion of the Nazca plate

Generally, examination of earthquakes along the Nazca-South America convergence margin of Chile's northern end of the central seismic region are indicative of the complexity in the moment release, which can be correlated to structural variations within the subducting and overriding plates. The anomalous interactions affect crustal displacements and, therefore, the source characteristics of tsunamis that can be generated from large-scale, thrust and reverse thrust seismic events in the region - nucleated by offshore compressional earthquakes (Pararas-Carayannis, 2010)

2. THE SATELLITE

The GOES-13 (Geostationary Operational Environmental Satellites) is a geosynchronous satellite situated at 36,000 km above the equator at 75° W longitude. The GOES satellites are three-axis stabilized, giving the Imager and Sounder a continuous view of the Earth. The Imager has a total of 22 detectors split into three groups: 1) Eight visible detectors, 2) Seven primary infrared detectors, and 3) Seven redundant infrared detectors. Each of the 22 detectors is a member of one of five spectral channels. Although physically distinct, the five channels are optically overlaid. For GVAR (GOES Variable) the uplink bit rate is 2000 bps at a frequency of 2034 Mhz. The IR detector data segment contains the scan line data for the associated detector. This segment varies in length directly with the scan line, reaching a maximum nominal length of 52,360 bits (5236 pixels) for a 19.2° wide scan. [NASA, 2015]. The scan mirror positioning for both instruments is controlled by two servo motors, one for the north-south elevation angle (outer gimbal motor) and one for the east-west scanning azimuth angle (inner gimbal motor). Errors may occur in the detector response characteristics due to aging and temperature variations in the instrument components. In addition, the IR detectors are subject to a low frequency random drift. Blackbody measurements are used to determine detector response characteristics, (specifically, gain and bias), based on an established relationship between blackbody temperature and equivalent target radiance as measured by each detector. The accuracy of the imager is 1 km for the visible detector and 4-8 km for the infrared detector.

In the following figure (Fig. 2) we show a satellite image taken by GOES-13 on 2015-9-16 at 23:08 UTC for the 10.7 μm channel

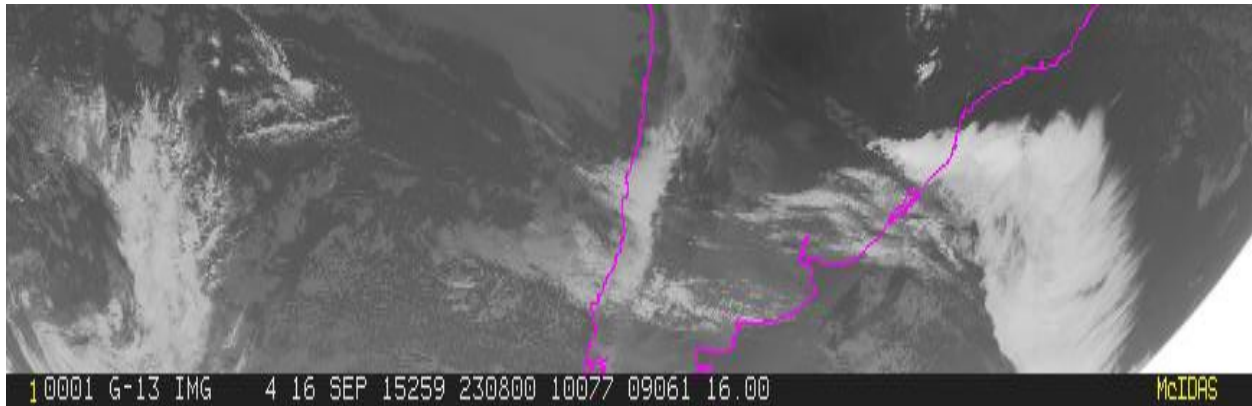


Fig.2: Goes-13 image for South America on 2015-9-16 at 23:08 UTC for the 10.7 μm channel

2. THE TSUNAMI RADIATION

In previous publications [Lin et al, 2010; Lin and Sookhanaphibarn, 2011; Lin et al., 2011; Lin et al., 2012; Lin et al., 2013; Lin et al., 2014, Lin et al, 2015] we have described the procedure by which a Signal Diagram can be extracted from the satellite image. Thus,

Algorithm 1:

begin

```
load(JPGfilename, Ytsunami , Xtsunami)
```

```
imageDat = imread(JPGfilename)
```

```
rowDat = imageDat(Ytsunami ; :)
```

```
columnDat = imageDat(:, Xtsunami)
```

```
return(rowDat, columnDat)
```

end

Here, *rowDat* is the latitudinal Signal Diagram and *columnDat* the longitudinal Signal Diagram. Y_t ; $X_{tsunami}$ are the coordinates of the earthquake epicenter, and *JPGfilename* refers to the satellite image. To assist investigators who might wish to reproduce or extend our work we are posting the complete MATLAB code in the Appendix.

For channel 1 the Signal Diagram is given below:

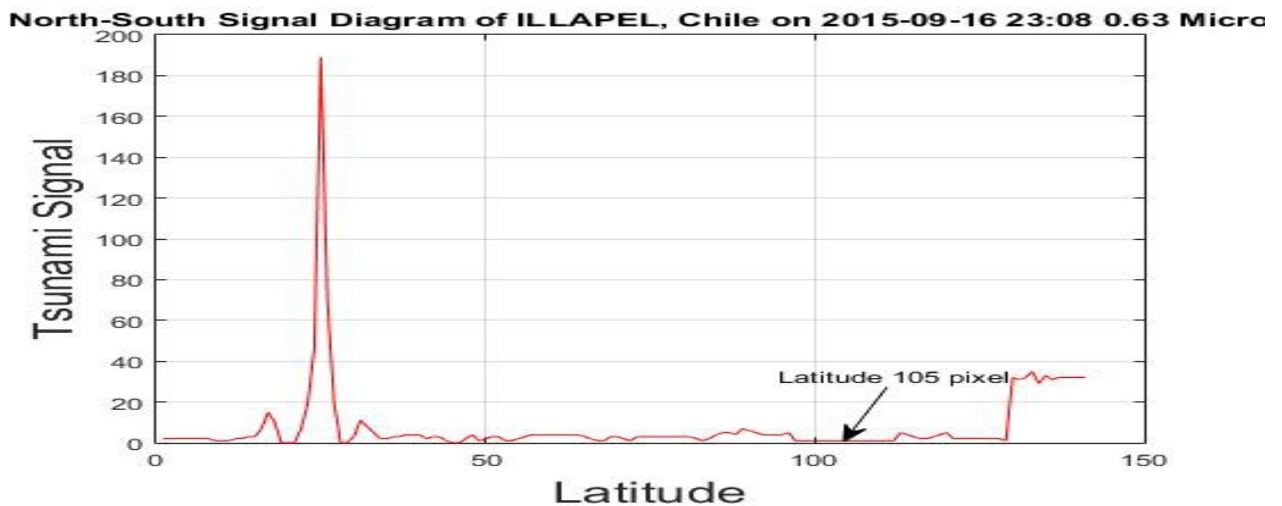


Fig.3: Longitudinal Signal Diagram on 2015-09-16 at 23:08 UTC for 0.63 μm

We observe that no signal was detected by GOES-13 at 23:08 UTC, which is 14 minutes after the 8.3 magnitude seaquake. This is due to the fact that the frequency 0.63 μm is in the visible spectrum, and the water molecules do not radiate at this frequency [Coudert *et al.*, 2004; Coudert, 1997; Toth, 1991; Toth, 1993]. Had it been otherwise, we would have observed the entire sky painted in red! Our experimental measurement therefore confirms theoretical expectation.

In Fig. 4 we show the Signal Diagram for channel 2 at 3.9 μm :

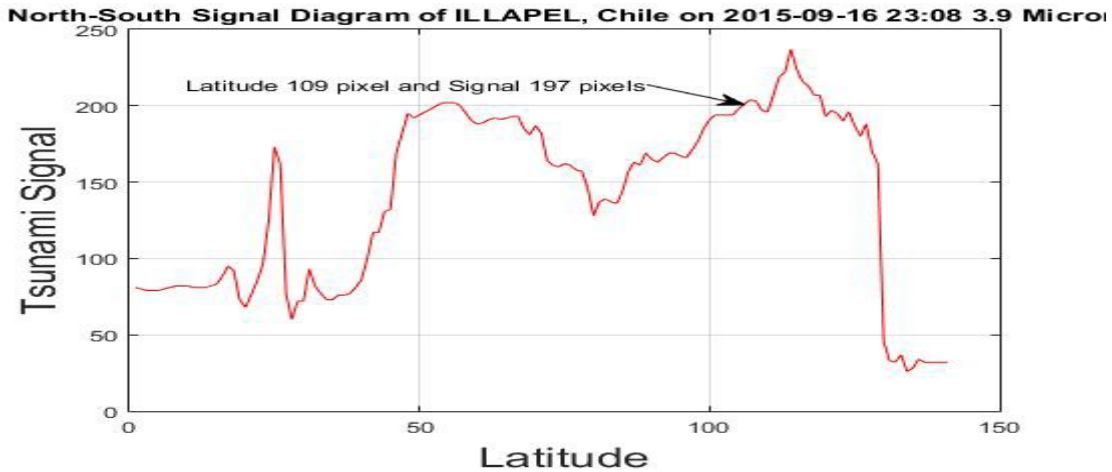


Fig.4: Longitudinal Signal Diagram on 2015-09-16 at 23:08 UTC for 3.9 μm

A Tsunami Signal of magnitude 197 pixels is observed. The intermediate infrared channel (IIR) at 3.9 μm belongs to the IR-C band in the infrared spectrum. This band is used for tracking purposes by heat seeking missiles. In the presence of a tsunami, therefore, a missile might be misdirected from its target.

In Fig 5 we show the Signal Diagram for channel 3 at 6.5 μm :

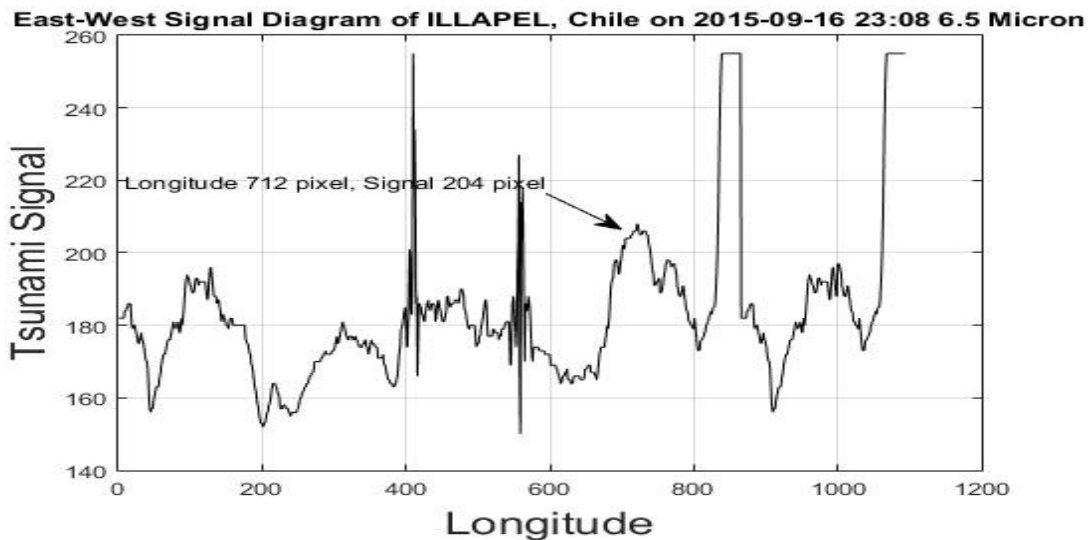


Fig.5: Latitudinal Signal Diagram on 2015-09-16 at 23:08 UTC for 6.5 μm

This is the Water Vapor channel which shows the amount of moisture in the air. As the moisture content of the air may vary greatly due to the action of wind, the tsunami signal may also fluctuate with time.

In Fig. 6 we show the Signal Diagram for channel 4 at 10.7 μm :

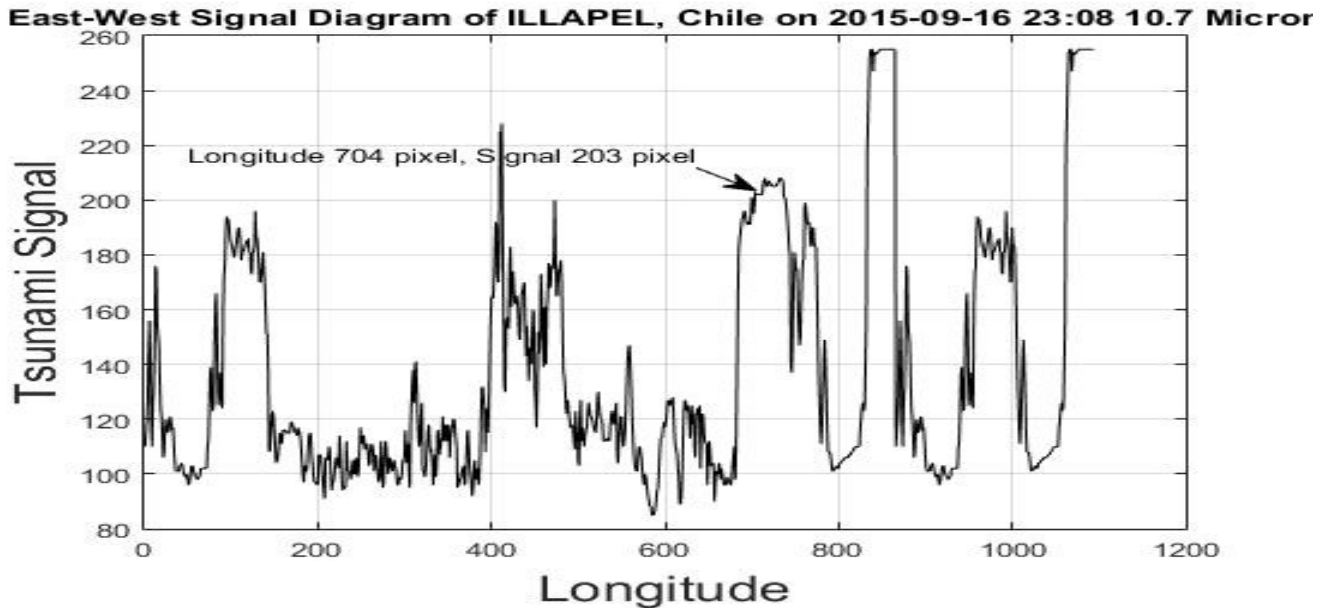


Fig.6: Latitudinal Signal Diagram on 2015-09-16 at 23:08 UTC for 10.7 μm

At this frequency, the Tsunami Signal is robust and we have utilized it in all of our previous investigations [Lin *et al.*, 2010; Lin and Sookhanaphibarn, 2011; Lin *et al.*, 2011; Lin *et al.*, 2012; Lin *et al.*, 2013; Lin *et al.*, 2014, Lin *et al.*, 2015]. The IR photon energy is between 0.001 and 1.7 eV.

This channel is the atmospheric window covered by detectors such as HgCdTe and microbolometers. Satellite images in this frequency region can be used to determine cloud heights and types, to calculate land and surface water temperatures, and to locate ocean surface features.

Finally, we show the Latitudinal Signal Diagram for channel 5 at 13.3 μm :

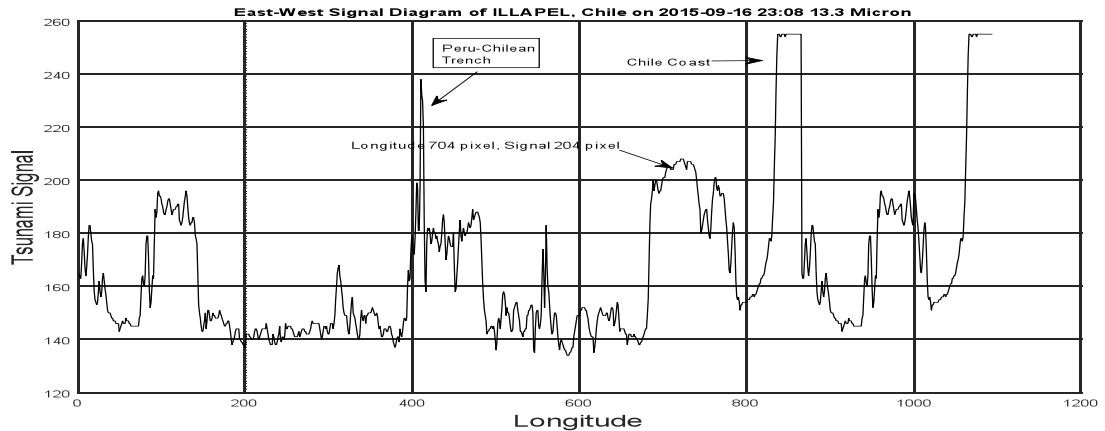


Fig.7: Latitudinal Signal Diagram on 2015-09-16 at 23:08 UTC for 13.3 μm

This Signal Diagram, which represents a slice across the satellite image along the latitude of the seaquake event from West to East, has two interesting features not so evident in the longitudinal Signal Diagrams: 1) the Tsunami Signal is very broad, extending approximately 25 pixels in width (corresponding to a terrestrial distance of about 100 km); 2) The Chilean coastline is clearly delineated, as pointed to by an arrow. Also of interest is that in all Latitudinal Signal Diagrams the enhanced radiation on the *subduction zone* from pixel = 400 up to 700 pixels is exhibited, as compared with the radiation emanating from the Pacific Ocean for pixel < 400 pixels. The Peru-Chilean trench is demarcated by a strong peak as pointed to by an arrow.

We summarize the above result in the following table: In this table we have also included the data measured at 23:38 UTC for comparison.

Table 1: Table of Tsunami Signals (S1, S2)*

channel	Image time 23:08 S ₁ pixels	Image time 23:38 S ₂	Mode	Remark
1. 0.63 μm	0.0	0.0	N/A	Cloud and surface features
2. 3.9 μm	197	194	Overtones, Combinatio	Low cloud, fog, fire
3. 6.5 μm	204	200	V ₂	WV
4. 10.7 μm	202	201	R,L1,L2	Surface/Cloud top temperature
5. 13.3 μm	206	201	R,L1,L2	Cloud heights

*The Longitudinal (North-South) Signal Diagrams are used for these measurements

The excitation of the water molecule can occur after multiple collisions. For a detailed analysis it is necessary to perform a quantum mechanical calculation for the transition probability of water molecule from the ground state to the excited state. Since the number of molecules participating in this event is of the order of 10^{36} [Lin et al, 2015], we expect that the radiation will be significant.

In previous work we have assumed that the tsunami eye extends to an area $10 \text{ km} * 10 \text{ km}$ and that the tsunami signal will subside within half an hour. Here, however, we have a case where the tsunami eye is $230 \text{ km} * 100 \text{ km}$ and the signal lasts for over an hour. We speculate that an observer navigating in the vicinity of the tsunami eye will be able to observe a gigantic cacophony of ‘*Son et lumière*’ show lasting over an hour, provided the observer wears a pair of infrared goggles. Indeed, the radiation will be observable in outer space, presumably by aliens.

On the molecular level, this radiation with wavelength $13.3 \mu\text{m}$ (751.9 cm^{-1}) corresponds to the rotational quantum level transition from (6 4 3) to the ground state (0 0 0) measured spectroscopically by Toth et al, who obtained a result of 756.7 cm^{-1} . [Toth,1991]. The discrepancy may be accounted for by the Coriolis Effect, the Centrifugal Effect, and above all, the Doppler Effect due to the high velocity of the molecules. Both the satellite measurement and the spectroscopic measurement are subject to experimental errors. For transitions at the other frequencies refer to [Lin et al; 2015]. The mode designates the type of motion executed by the water molecule in its excited state before transition to the ground state by emitting a photon.

3. CONCLUSION

We hypothesize that a seaquake with magnitude greater than 7.0 will generate a tsunami accompanied by multispectral radiation in the infrared domain. Previous studies [Lin et al, 2010; Lin and Sookhanaphibarn, 2011; Lin et al., 2011; Lin et al., 2012; Lin et al., 2013; Lin et al., 2014, Lin et al, 2015] confirm that this is indeed the case for Banda Aceh (2004), Tohoku (2011), N. Sumatra (2011), and Sulangan (2012). Two cases, Bio-Bio (2010) and Ofunato (2012) have issues that are not definitively resolved, but do not constitute counter-examples. The present investigation reaffirms the validity of our hypotheses. We detected infrared radiation at the following wavelengths: $3.9 \mu\text{m}$, $6.5 \mu\text{m}$, $10.7 \mu\text{m}$, and $13.3 \mu\text{m}$. No radiation is detected at $0.63 \mu\text{m}$, which is in the visible spectrum. The Tsunami Signals that we have observed did not decay within 44 minutes. This is probably related to the exceptionally huge size of the tsunami eye. The radiation at $13.3 \mu\text{m}$ corresponds to the rotational quantum level transition from (6 4 3) to the ground state (0 0 0). We note that the elevated temperature and the high speed of the molecules in a tsunami are energetically capable of stimulating the molecules to excited quantum energy levels by collisions.

REFERENCES

- [USGS,2015] http://earthquake.usgs.gov/earthquakes/eventpage/us20003k7a#general_summary
Retrieved September 16, 2015
- [Wikipedia,2015]
https://en.wikipedia.org/wiki/2015_Illapel_earthquake
- [NASA,2015] <http://goes.gsfc.nasa.gov/text/GVARRDL98.pdf>
- Coudert, L.H., 1994. Analysis of the Rotational Levels of Water and Determination of the Potential Energy Function for the Bending ν_2 Mode: J. of Mol. Spectroscopy 165, pp.406-425.
- Coudert, L.H., 1997. Analysis of the Line Positions and Line Intensities in the ν_2 Band of the Water Molecule: J. of Mol. Spectroscopy 181, pp.246-273
- Coudert, L.H., O.Pirali, M.Vervloet, R.Languetin and C.Camy-Peyret, 2004. The eight first vibrational states of the water molecule: measurement and analysis. J. of Molecular Spectroscopy 228, pp. 471-498.
- Lanquetin, R., L.H.Coudert and C.Camy-Peyret, 1999. High-Lying Rotational Levels of Water: Comparison of Calculated and Experimental Energy Levels for (0 0 0) and (0 1 0) up to $J=25$ and 21. J. of Mol. Spectroscopy 195, 54-67.
- Lanquetin, R., L.H.Coudert and C.Camy-Peyret, 2001. High-Lying Rotational Levels of Water: An Analysis of the Energy Levels of the Five Vibrational States: J. of Mol. Spectroscopy 206, 83- 103.
- Lin F.C., K. Na Nakornphanom, K. Sookhanaphibarn, and C. Lursinsap, 2010.“A New Paradigm for Detecting Tsunamis by Remote Sensing”; International Journal of Geoinformatics, Vol.6, No.1, March 2010, pp.19-30.
- Lin F.C. and K. Sookhanaphibarn, 2011. Representation of Tsunamis in Generalized Hyperspace: Proceedings of the IEEE International Geoscience and Remote Sensing Symposium (IGARSS'11), Sendai/Vancouver, July 21, 2011. pp. 4355-4358.
- Lin F.C., W. Zhu and K. Sookhanaphibarn, 2011. Observation of Tsunami Radiation at Tohoku by Remote Sensing, Science of Tsunami Hazards, Vol.30, No.4,Honolulu, HI, December 2011, pp. 223-232.
- Lin, F.C., W. Zhu and K. Sookhanaphibarn, 2012. A Detail Analysis of the Tohoku Tsunami by Remote Sensing, Proceedings of the IEEE International Geoscience and Remote Sensing Symposium (IGARSS'12), Munich, Germany, pp.1166-1169.
- Lin. F.C., W. Zhu, K. Sookhanaphibarn and P. Silapasuphakornwong, 2013. REMOTE:-A Satellite Based Tsunami Early Warning Detection System, Proceedings of the IEEE International Geoscience and Remote Sensing Symposium (IGARSS' 13), Melbourne, Australia, pp. 3694- 3697.

Lin, F.C., K. Sookhanaphibarn, V. Sa-yakanit and G. Pararas-Carayannis, 2014. REMOTE: Reconnaissance & Monitoring of Tsunami Events, Science of Tsunami Hazards, Vol.33, No.2, pp.86-111

Lin, F.C., K.Sookhanaphibarn, W. Choensawat and G. Pararas-Carayannis: On the Frequency Spectrum of Tsunami Radiation, Science of Tsunami Hazards, Vol.34, No.3, pp.34

Martin, W.C. and W.L.Wiese, 1996. Atomic, Molecular and Optical Physics Handbook, G.W.R.Drake, Ed., AIP Press, Woodbury, N.Y.

Pararas-Carayannis, G., 2010. The earthquake and tsunami of 27 february 2010 in Chile – Evaluation of Source Mechanism and of Near and Far-field Tsunami Effects. Science of Tsunami Hazards, Vol. 29, No. 2, pp 96 - 126 (2010)

Pararas-Carayannis, G., 2012. Geodynamics of Nazca ridge's oblique subduction and migration - implications for tsunami generation along central and southern Peru: Earthquake and Tsunami of 23 June 2001. Science of Tsunami Hazards, Vol 31, No. 2, pp. 129-153, 2012

Pararas-Carayannis, G., 2013. "The Great Tohoku-Oki Earthquake and Tsunami of March 11, 2011 in Japan: A Critical Review and Evaluation of the Tsunami Source Mechanism," Pure and Applied Geophysics, pp. 1-22.

Tennyson, J., N.F. Zobov, R. Williamson, O.L. Polyansky, P.F. Bernath, 2001. Experimental energy levels of the water molecule. Journal of Physical and Chemical Reference Data, 30 (3). pp. 735- 831.

Toth, R. A., 1991. ν_2 band of H₂O: line strengths and transition frequencies. J. Opt. Soc. Am. B, Vol.8, No.11, November 1991, pp.2236-2255.

Toth, Robert A., 1993. $2\nu_2 - \nu_2$ and $2\nu_2$ bands of H₂O, H₂¹⁷O and H₂¹⁸O: Line Positions and Strength: J. Opt. Soc. Am. B, Vol.10, No.9, September 1993, pp. 1526-1544.

APPENDIX

```
%mainTsunamiDetection6.m
% Clear parameters and close all windows
%clear
clc
close all
warning('off','MATLAB:dispatcher:InexactCaseMatch');
% INPUT FILES
%display(' Please enter TITLE, such as 'TOHOKU 2011-3-11 06:30 UTC');
%TITLE = input('Please enter TITLE of this project in quotes;e.g. TOHOKU DATE
of image,TIME UTC: ');
JPGfilename= input('input image name e.g."COUNTRY_GOES_IMAGE.jpg: " ');
%display(' Please enter JPG filename for satellite image:');
%display(' ');
%display(' ');
REFfilename= 'Country_mainshock_ref.tex';
%REFfilename=input('INPUT the file for three reference points to be read into
MATLAB:', 's');
%display(' Please enter latitude & longitude of three reference points and
their pixel values:');
% Note
% Range for Deletion = 75:220

% Main Procedure
fopen(JPGfilename);
ReadJPG( JPGfilename );
%clear command window;
[X_tsunami, Y_tsunami]=calculatePixelForEarthquake6(REFfilename);
rowDat =
extractRowDatMainshock6(JPGfilename,round(Y_tsunami),round(X_tsunami));
display('Now write TITLE,save signal diagram,workspace,and press enter to call
WAVEMENU:');
pause;
wavemenu;
% Use 1D signal, import signal, and do Analysis:
% This is the end of the Program

function [X_tsunami, Y_tsunami]=calculatePixelForEarthquake6(~)
%calculatePixelForEarthquake6.m
fid = fopen('Country_mainshock_ref.tex');
tline = fgetl(fid);
display('Enter the pixel values of A and B and the earthquake position:');
display('NOTE:The southern or Western hemisphere,longitude and latitude may be
negative.');
```

```
disp('ACHTUNG. For A,B and earthquake epicenter --');
disp('all latitudes and longitudes must have the same sign.');
```

```
beep on;
disp('In northern hemispere, CHOOSE lat A < lat of epicenter and lat B > lat
of epic: ');
```

```

disp('Choose long A < long of epic and long B > long of epic. ');
disp('Ditto in southern hemisphere. lat and long of A must be less than those
of epicenter and B. ');
disp('A and B must enclose earthquake epicenter. ');
display(datestr(now));
pause(5);
beep off;
while ischar(tline)
    tline = fgetl(fid);
    if (tline(1)==' ')
        display(' ');
    elseif (~isempty(strfind(tline,'RefA_Xco')))
        RefA_Xco=str2num(tline(strfind(tline,'=')+1:length(tline)));
    elseif (~isempty(strfind(tline,'RefA_Yco')))
        RefA_Yco=str2num(tline(strfind(tline,'=')+1:length(tline)));
    elseif (~isempty(strfind(tline,'RefB_Xco')))
        RefB_Xco=str2num(tline(strfind(tline,'=')+1:length(tline)));
    elseif (~isempty(strfind(tline,'RefB_Yco')))
        RefB_Yco=str2num(tline(strfind(tline,'=')+1:length(tline)));
    % elseif (~isempty(strfind(tline,'RefC_Xco')))
    %     RefC_Xco=str2num(tline(strfind(tline,'=')+1:length(tline)));
    % elseif (~isempty(strfind(tline,'RefC_Yco')))
    %     RefC_Yco=str2num(tline(strfind(tline,'=')+1:length(tline)));
    elseif (~isempty(strfind(tline,'RefA_Lat')))
        RefA_Lat=str2num(tline(strfind(tline,'=')+1:length(tline)));
    elseif (~isempty(strfind(tline,'RefA_Lon')))
        RefA_Lon=str2num(tline(strfind(tline,'=')+1:length(tline)));
    elseif (~isempty(strfind(tline,'RefB_Lat')))
        RefB_Lat=str2num(tline(strfind(tline,'=')+1:length(tline)));
    elseif (~isempty(strfind(tline,'RefB_Lon')))
        RefB_Lon=str2num(tline(strfind(tline,'=')+1:length(tline)));
    % elseif (~isempty(strfind(tline,'RefC_Lat')))
    %     RefC_Lat=str2num(tline(strfind(tline,'=')+1:length(tline)));
    % elseif (~isempty(strfind(tline,'RefC_Lon')))
    %     RefC_Lon=str2num(tline(strfind(tline,'=')+1:length(tline)));
    elseif (~isempty(strfind(tline,'Lat')))
        Lat=str2num(tline(strfind(tline,'=')+1:length(tline)));
    elseif (~isempty(strfind(tline,'Lon')))
        Lon=str2num(tline(strfind(tline,'=')+1:length(tline)));
    else disp(' ');
    end
end
fclose(fid);
%NOTE! the longitude increses from east to westin the eastern hemisphere,
while the pixel value
%decreases from east to west:
%NOTE: the latitude increases from north to south in the northern hemisphere;
while the pixel value
%decreases from north to south.

```

```

%The latitude in the southern hemisphere is negative;
%The longitude in the western hemisphere is negative.
reply = input('Are the geodectics all in the northern hemisphere? (y/n): ',
's');

if strcmp(reply,'y')
    disp(reply)
end
if reply == 'y' %true
if Lon > RefA_Lon
    X_tsunami=abs(abs((abs(Lon-RefA_Lon)/abs(RefB_Lon-RefA_Lon))*abs(RefB_Xco-
RefA_Xco)+abs(RefA_Xco)));%end%longitude pix decreases from C
end
if Lat > RefA_Lat
    Dgeo=abs(Lat - RefA_Lat);
    A2Bgeo=abs(RefA_Lat-RefB_Lat);
    A2Bpix=abs(RefA_Yco-RefB_Yco);
    Dpix=A2Bpix*Dgeo/A2Bgeo;
    Y_tsunami=RefA_Yco-abs(Dpix);
end
    % Y_tsunami=abs(abs((abs(Lat-RefA_Lat)/abs(RefB_Lat-RefA_Lat))*abs(RefB_Yco-
RefA_Yco)+abs(RefA_Yco)));%lat pixel increases from A

if Lat < RefA_Lat
    Dgeo=abs(Lat - RefA_Lat);
    A2Bgeo=abs(RefA_Lat-RefB_Lat);
    A2Bpix=abs(RefA_Yco-RefB_Yco);
    Dpix=A2Bpix*Dgeo/A2Bgeo;
    Y_tsunami=RefA_Yco+abs(Dpix);
%Y_tsunami=abs(abs((abs(Lat-RefA_Lat)/abs(RefB_Lat-RefA_Lat))*abs(RefB_Yco-
RefA_Yco)-abs(RefA_Yco)));%lat pixel decreases from A
end

if Lon < RefA_Lon
    Dgeo=abs(Lon - RefA_Lon);
    A2Bgeo=abs(RefA_Lon-RefB_Lon);
    A2Bpix=abs(RefA_Xco-RefB_Xco);
    Dpix=A2Bpix*Dgeo/A2Bgeo;
    X_tsunami=RefA_Xco-abs(Dpix);
    %X_tsunami=abs(abs((abs(Lon-RefA_Lon)/abs(RefB_Lon-RefA_Lon))*abs(RefB_Xco-
RefA_Xco)-abs(RefA_Xco)));
end

if reply == 'n' % false
    if Lon > RefA_Lon
        Dgeo=abs(Lon - RefA_Lon);
        A2Bgeo=abs(RefA_Lon-RefB_Lon);
        A2Bpix=abs(RefA_Xco-RefB_Xco);
        Dpix=A2Bpix*Dgeo/A2Bgeo;
        X_tsunami=RefA_Xco+abs(Dpix);
    
```

```

% X_tsunami=abs(abs((abs(Lon-RefA_Lon)/abs(RefB_Lon-
RefA_Lon))*abs(RefB_Xco-RefA_Xco)+abs(RefA_Xco)));%end%longitude pix decreases
from C
end
if Lat > RefA_Lat
Dgeo=abs(Lat - RefA_Lat);
A2Bgeo=abs(RefA_Lat-RefB_Lat);
A2Bpix=abs(RefA_Yco-RefB_Yco);
Dpix=A2Bpix*Dgeo/A2Bgeo;
Y_tsunami=RefA_Yco-abs(Dpix);
end
% Y_tsunami=abs(abs((abs(Lat-RefA_Lat)/abs(RefB_Lat-
RefA_Lat))*abs(RefB_Yco-RefA_Yco)+abs(RefA_Yco)));%lat pixel increases from A

if Lat < RefA_Lat
Dgeo=abs(Lat - RefA_Lat);
A2Bgeo=abs(RefA_Lat-RefB_Lat);
A2Bpix=abs(RefA_Yco-RefB_Yco);
Dpix=A2Bpix*Dgeo/A2Bgeo;
Y_tsunami=RefA_Yco+abs(Dpix);
%Y_tsunami=abs(abs((abs(Lat-RefA_Lat)/abs(RefB_Lat-RefA_Lat))*abs(RefB_Yco-
RefA_Yco)-abs(RefA_Yco)));%lat pixel decreases from A
end

if Lon < RefA_Lon
Dgeo=abs(Lon - RefA_Lon);
A2Bgeo=abs(RefA_Lon-RefB_Lon);
A2Bpix=abs(RefA_Xco-RefB_Xco);
Dpix=A2Bpix*Dgeo/A2Bgeo;
X_tsunami=RefA_Xco-abs(Dpix);
%X_tsunami=abs(abs((abs(Lon-RefA_Lon)/abs(RefB_Lon-RefA_Lon))*abs(RefB_Xco-
RefA_Xco)-abs(RefA_Xco)));
end
end

display(X_tsunami);

display(Y_tsunami);

pause(5);

end

function rowDat = extractRowDatMainShock6(JPGfilename,Y_tsunami,X_tsunami)
%load(JPGfilename);
imageFile=imread(JPGfilename);

im = imageFile;
rowDat = im(Y_tsunami,:);
columnDat = im(:,X_tsunami);

```

```

pause on;

pause(2);
%plot(1:length(rowDat),rowDat);
x=1:length(rowDat);
y=1:length(columnDat);
figure, grid on;
title('East-West Signal Diagram');
plot(x,rowDat,'k');
ylabel('Tsunami Signal','FontSize',18);
xlabel('Longitude','FontSize',18);
%PLOTTOOLS;

low=input('Input the range of X-pixels for deletion (starting point) :');

u=input('Input the range of X-pixels for deletion (ending point) :');
pause(1);
rowDat(low:u)=[];
%legend(TITLE);
x=1:length(rowDat);
figure, plot(x,rowDat,'k');
ylabel('Tsunami Signal','FontSize',18);
xlabel('Longitude','FontSize',18);
grid;
pause(10);

disp('Now plot columnDat. ');
pause(10);
figure, title('North-South Signal Diagram');
plot(y,columnDat,'r');
grid;
ylabel('Tsunami Signal','FontSize',18);
xlabel('Latitude','FontSize',18);
%disp('Press Enter to continue:');
%low=input('Input the range of X-pixels for deletion (starting point) :');
%u=input('Input the range of X-pixels for deletion (ending point) :');
pause(3);
%close(h);
disp('EW Tsunami Signal = ');
disp(rowDat);
disp('NS Tsunami Signal = ');
disp(columnDat);
%pause off;
%saveFile=strrep(rowDat, '.jpg', '.mat');
%eval(['save ' saveFile ' rowDat']);
disp('Y value of earthquake:Y_tsunami= ');disp(Y_tsunami);
disp('X value of earthquake:X_tsunami= ');disp(X_tsunami);

```

```

S=max(rowDat);
disp('Max value of EW signal is:');disp(S);

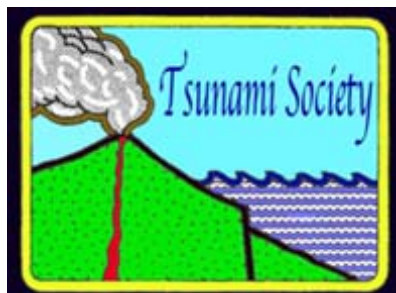
%Goto wavemenu for Signal Diagram importing signal from workspace, using 1D
wavelet
%
%figure;
%plot(rowDat); hold on;
%GRID;
%text(xLoc,double(rowDat(xLoc))+20,'\leftarrow ','FontSize',18);
%Title;
hold off;
pause(5);
%figure;
%plot(columnDat); hold on;
%GRID;
%ylabel('Tsunami Signal','FontSize',18);
%xlabel('Latitude','FontSize',18);
hold off;
display('wavemenu starts;USE IMPORT "ANS" FROM WORKSPACE FOR SIGNAL. ');
pause(3);
%USE IMPORT "ANS" FROM WORKSPACE FOR SIGNAL
%Copyright:Kingkarn Sookhanaphibarn & Frank C Lin
end

```

```

function ReadJPG( JPGfilename )
%Read a JPG file into MATLAB
a=imread(JPGfilename,'jpg');
imtool(a);
end

```



SCIENCE OF TSUNAMI HAZARDS

Journal of Tsunami Society International

Volume 35

Number 1

2016

**THE ECONOMIC EVALUATION AND SIGNIFICANCE OF AN EARLY RELOCATION
VERSUS COMPLETE DESTRUCTION BY A POTENTIAL TSUNAMI OF A COASTAL CITY IN
ECUADOR**

**Fabian Rodriguez, Mario Cruz D'Howitt, Theofilos Toulkeridis*, Rodolfo Salazar,
Gioconda Elizabeth Ramos Romero, Veleria Alejandra Recalde Moya and Oswaldo
Padilla**

Universidad de las Fuerzas Armadas ESPE, Sangolquí, Ecuador

• Corresponding author: ttoulkeridis@espe.edu.ec or theousfq@yahoo.com

•
ABSTRACT

The coastal part of continental Ecuador is highly vulnerable for tsunami hazards as shown in the past two centuries. In order to avoid future devastating destructions in a given part in the coastline, we have estimated the economic effects of a potential future tsunami for one small Pacific town in Ecuador in order to analyze such potential cost of damages and compare it with a proposed resettlement value of the entire town. In past, most of the known resettlement projects have been realized as result of a natural disaster or a planning infrastructure such as hydro-electrical plants. Yet, in this study, we have considered to propose to policy makers and other authorities to take into account that a resettlement plan should be realized prior an impact by one the most deadly natural hazard. The results include four different scenarios of economic losses as a result of a potential tsunami, using human losses as the only variable that vary. Potential economic losses vary from 441 US\$ up to 620 US\$ millions, when compared to a potential resettlement and associated costs based on the four scenarios. The B/C ratio is favorable to town resettlement as Government's preventing policy favoring an intelligent reduction and prevention of vulnerability and loss of human life.

Key words: Tsunami, Economic loss, Resettlement, Prevention, Ecuador

1. INTRODUCTION

Among earthquakes and floods, tsunamis are one of the most destructive and deadliest natural hazards (Raschky, 2008; Daniell et al., 2010). In recent years many studies have been performed to demonstrate and evaluate the vulnerability of coastal cities, their entire strategic infrastructure and their habitants towards the impact of tsunamis and other associated natural occurring hazards of one or multiple origins (González-Riancho et al., 2015). Four prominent examples of the last dozen of years in Indonesia, Chile and Japan, demonstrate such issue. The 2004 tsunami with a magnitude of 9,3 struck in Indonesia and surrounding countries causing 350,000 deaths and 15 billion US\$ of immediately economic lost (Athukorala and Resosudarmo, 2005; Jayatilleke and Naranpanawa, 2007). The most prominent example may be the case of Japans 9,0 magnitude tsunami of 2011, where besides the 15,853 deaths, 6,023 injured and 3,282 missing people some 300,000 building were destroyed, while 4,000 roads, 78 bridges and 29 railways were severely affected (National Police Agency of Japan, 2015). The economic damage reached approximately 210 billion US\$ of which 66.9 billion were insured lost (Aon Benfield, 2015). Similarly, the 8.8 magnitude tsunami struck in Concepción, Chile in 2010, with a catastrophic effect throughout the country, with some 500 deceased and at least 1,5 million homes damaged of which one third were completely destroyed, leaving an economic loss of approximately 30 billion US\$, of which 8,5 billion insured lost (Barcená et al., 2010). Later in 2015, in the same country another 8,3 magnitude tsunami hit offshore of Coquimbo, with an estimated economic loss between 100 million US\$ up to 1 billion US\$ (USGS, 2015).

Based on the four demonstrated examples it is obvious, that the consequences of any tsunami impact certainly become an economic devastation for any region or city along the coasts worldwide. Therefore, better preventive educational activities and in some cases the construction of mitigation structures supported risk reduction or at least the acceptance of minor remaining risks (González-Riancho et al., 2015). Nonetheless, due to the enormous financial damage a community resettlement should be also considered as part of a plausible mitigation plan. Resettlement requires a careful and detailed planning (English and Brusberg, 2002). A resettlement process implies displacement of human population, where disturbance is calculated as it affects housing, employment, commerce and also ways of living (World Bank, 2004).

However, if damage costs are overwhelming higher than relocation of an entire town, than state or even local governments should consider resettlement as an alternative before certain future disasters take place. The main objective of our study therefore is, to present new data and calculations of how a major strike of a future tsunami may be prevented by a simple relocation of a small city in coastal Ecuador, which may be considered as a pioneer example to be followed.

2. GEODYNAMIC SETTING AND PROBABILITY OF TSUNAMIS

Due to its active geodynamics the Ecuadorian continental platform similar to almost all other countries along the Pacific Rim is a frequent target of tsunami impacts (Gusiakov, 2005; Pararas-Carayannis, 2012). The active continental margin and associated subduction zone between the oceanic Nazca Plate with the continental South American and Caribbean Plates, both separated by the Guayaquil-Caracas Mega Shear (Kellogg and Vega, 1995; Gutscher et al., 1999; Egbue and Kellogg, 2010) give rise to tsunamis of tectonic as well submarine landslide origin (Shepperd and

Moberly, 1981; Pontoise and Monfret, 2004; Ratzov et al, 2007; 2010; Ioualalen et al., 2011; Pararas-Carayannis, 2012). A further origin if tsunamis have been credited to the Galápagos volcanism (Toulkeridis, 2011). The active Galápagos hotspot has produced several voluminous shield-volcanoes, most of which are inactive due to the ESE-movement of the overlying Nazca oceanic plate (Holden and Dietz 1972; Toulkeridis, 2011). The main Galápagos Islands are located south of the E-W-trending Galápagos Spreading Center, east of the N-S-trending East Pacific Rise and some 1000 km west of the Ecuadorian mainland. Due to the volcanic activity and the subsequent plate drifting, two aseismic volcanic ridges were created. The first being the Cocos Ridge is moving to the NE while the second, being the Carnegie Ridge is moving to the East above the Cocos and Nazca Plates, respectively (Harpp et al., 2003). These submarine extinct volcanic ridges are the result of cooling/contraction reactions of magma, as they slowly sunk below the sea surface due to the lack of magma supply, lithospheric movement and strong erosional processes. With time, these submarine volcanic ridges as well as various microplates, have accreted on the South American continent (Reynaud et al., 1999; Harpp and White, 2001). Nonetheless, such aseismic ridges like the Carnegie Ridge become and obstacle in the oblique subduction process and may generate within the subduction zone a potential valve of tsunamis along the Ecuadorian coast (Pararas-Carayannis, 2012). The Carnegie Ridge collides towards the Ecuadorian continental margin with a velocity of as low as 5 cm per year at a latitude between 1°N and 2°S (Pilger, 1983). Further local tsunamis may be generated by seismotectonic extensional processes in some areas along the Ecuadorian coast like in the Gulf of Guayaquil besides other zones (Pararas-Carayannis, 2012).

From the known record, the Ecuadorian shoreline has witnessed a dozen times impacts of tsunamis by mainly local origins in the last two centuries with various intensities one being of up to 8.8 Mw in 1906 (Rudolph and Szirtes, 1911; Kelleher, 1972; Beck and Ruff, 1984; Kanamori and McNally, 1982; Swenson and Beck, 1996; Pararas-Carayannis, 2012), while evidences of paleo-tsunami deposits are scarce (Chunga and Toulkeridis, 2014). Other prominent examples of tsunamis along the Ecuador–Colombia subduction zone include tsunamis in 1942 (Mw=7.8), 1958 (Mw=7.7) and 1979 (Mw=8.2) within the 600-km long rupture area of the great 1906 event (Collot et al., 2004). While the 1906 event caused the death of up to 1500 persons in Ecuador and Colombia with an unknown financial damage to the existing infrastructure, the 1979 tsunami killed in Colombia at least 807 persons and destroyed approximately 10,000 homes, knocking out electric power and telephone lines (Pararas-Carayannis, 1980).

The evaluation of the last marine quakes, which generated tsunamis, suggests that the probability of a major or great earthquake in this margin region is enormous, especially as there must be substantial strain accumulation in this region (Pararas-Carayannis, 2012). Additionally, given into consideration that the last earthquake in 1979 did not release the amount of energy as the 1906 event, there is a high probability in the near future, that an earthquake within the Ecuadorian-Colombian trench may generate a tsunami of similar magnitude to that of 1906, which might be even more destructive than the one in the past if it occurs near high tide (Pararas-Carayannis, 2012). The potential of high losses and damage is given by the fact that the infrastructure of the fishing, tourism and other industries and the movement to live along the beaches, have been highly developed within the last decades along the Ecuadorian coasts. Based on historic know tsunamis in Ecuador of the last two centuries, the probability of a strike in 2015 is of about 87%.

The village of San Vicente in central Manabí Province is exclusively composed by quaternary sediments of the so-called Canoa formation (Bianucci et al., 1997) and is situated along the Ecuador–Colombia subduction zone, exactly east of the W-E striking Carnegie Ridge at a latitude of 0.35°S (Fig. 1). This region is being highly vulnerable to tsunamis, flooding, landslides and mud flows (Cruz D' Howitt et al., 2010).

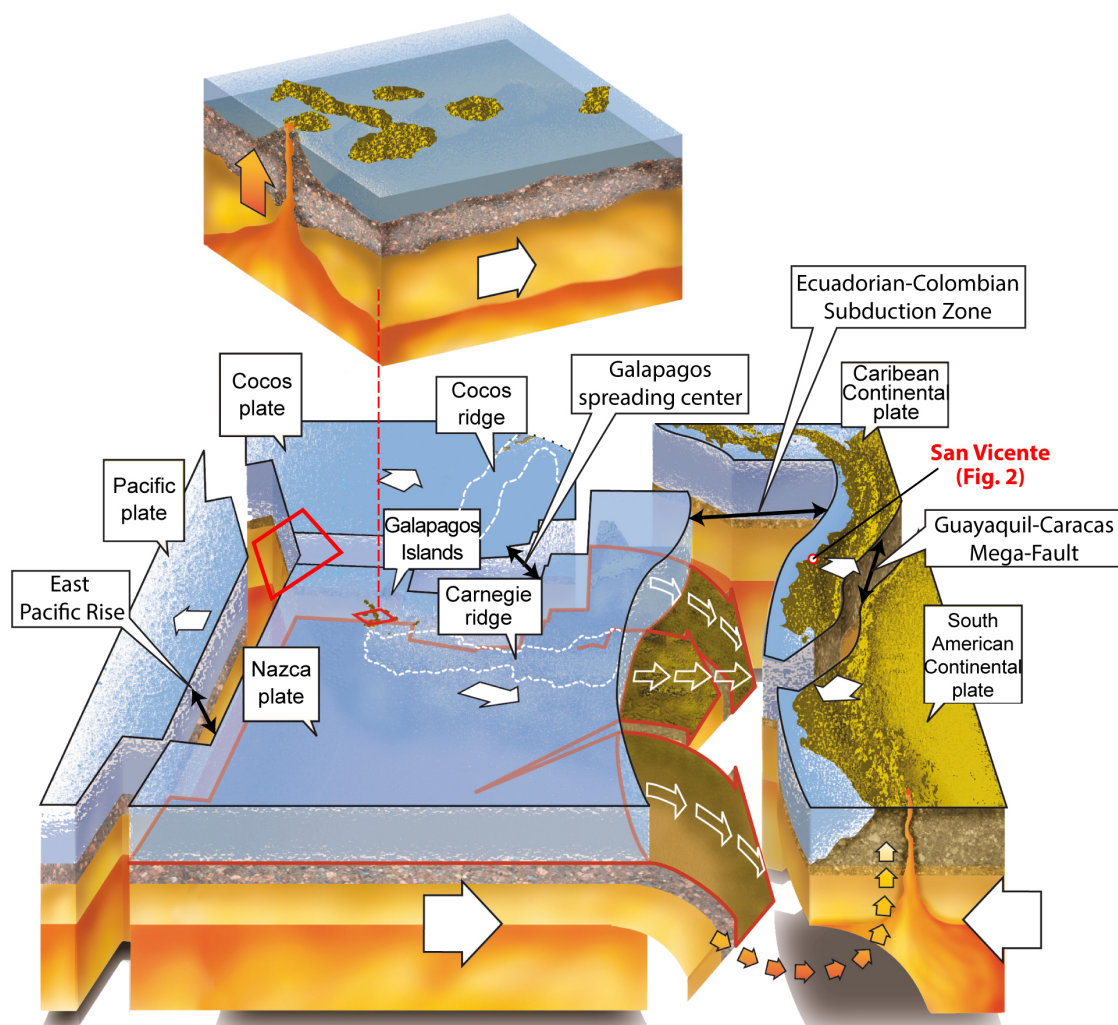


Figure 1: Geodynamic setting of Ecuador, the Galapagos Islands and the Carnegie Ridge. Adapted from Toulkeridis, 2013

3. METHODOLOGY

3.1 Mapping

The region around San Vicente, an area of approximate 33 km² (urban area), has been classically field-mapped and additionally interpreted by air photography evaluation. The resulting hazard maps are focused on tsunamis, landslides and mudflows as well as flooding by overflow of

rivers and eventual high precipitation rates. All potential hazards besides the tsunami impact have been overlapped in a multi-hazard map (Fig. 2).

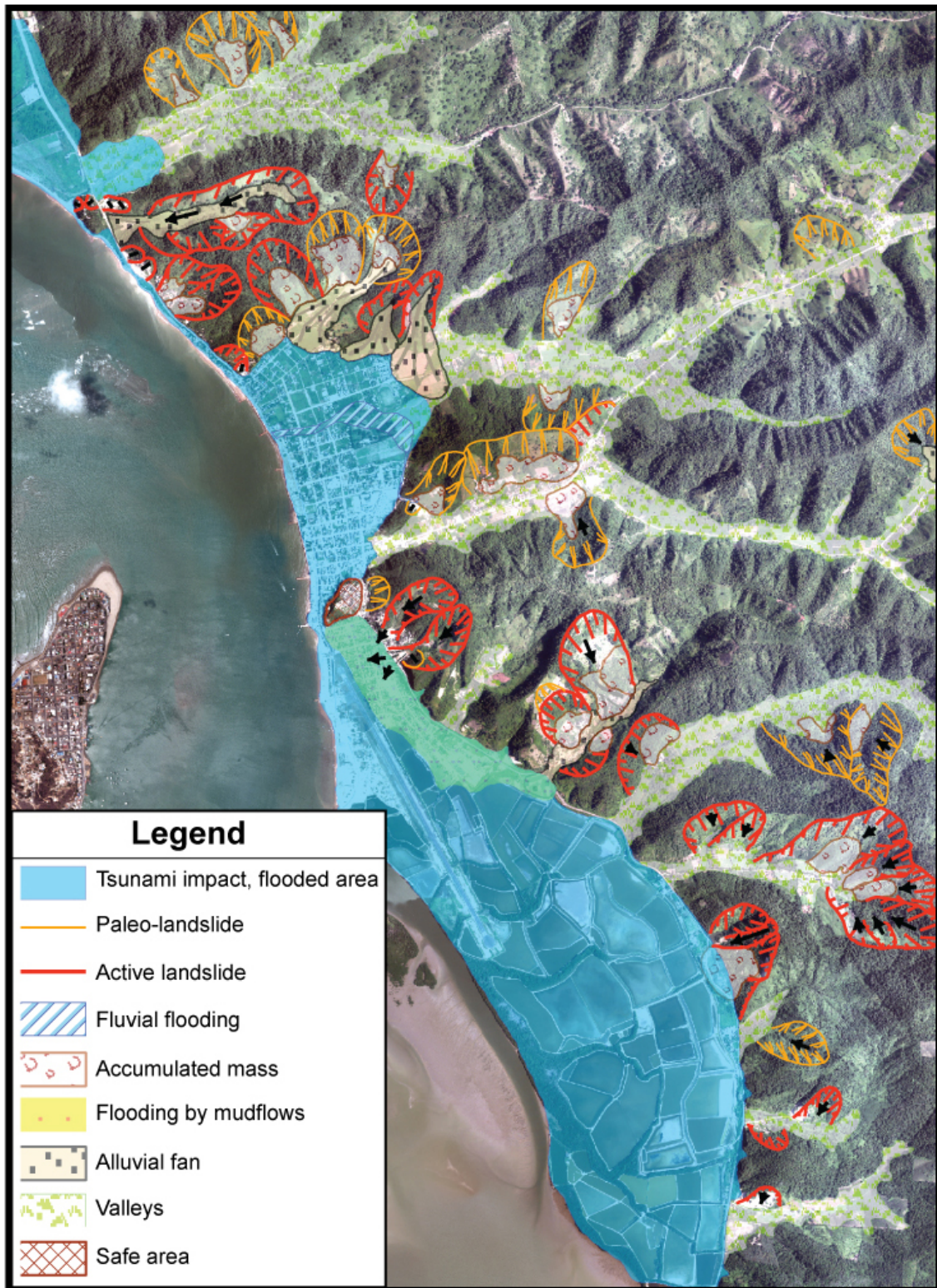


Figure 2: Multi-hazard map of San Vicente area

3.2 Calculating the cost of involvement for each hazard type

In order to know the specific value of each lot, the value has been calculated per square meter of each lot in accordance with its corresponding zoning. The value per square meter of each lot has been calculated pending and according to the area where it has been located. This value has been stored it in the field “damage_square meter”. With this coverage and by using ArcGIS Spatial Analyst the Intersect operation was performed with the areas (shapes) of alluvial fans, mudflows, and river flooding and flooding by tsunamis. This allowed identifying the lots affected by each mentioned hazard. With each calculated cover, two additional fields were generated. First is the area (area_square meter) and second is the damage (damage_square meters per area). Damage was calculated by the cost of the damage multiplied with area involved or affected. This resulted to an addition of all values leading to the final sum of economic damage by all hazards. All steps are illustrated in Fig. 3.

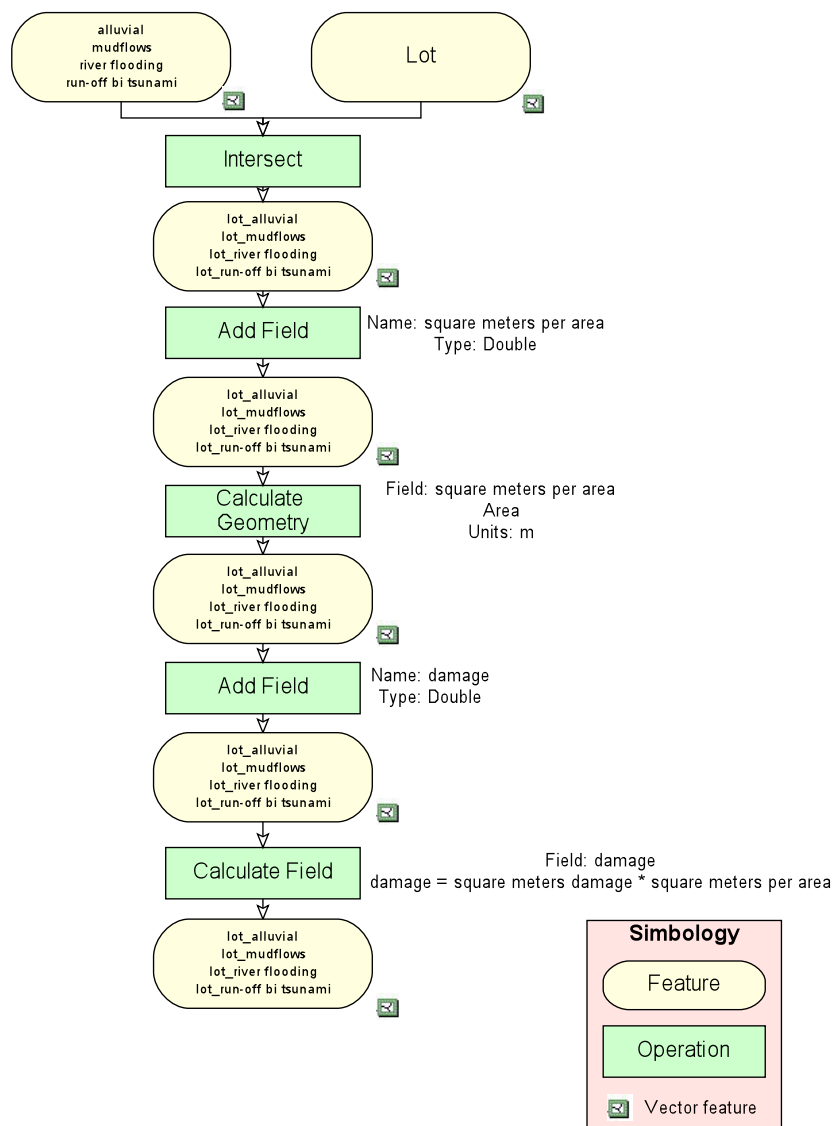


Figure 3: Sketch of all operations leading to the calculation of the costs produced by the damage of a variety of hazards in the San Vicente area.

On the other hand, the theoretical framework that encompasses economic analysis of a potential tsunami in San Vicente is the cost benefit analysis (BCA) which is used to evaluate financial consequences of decision making and its main objective is to increase public welfare (Zerbe et al., 2010). Benefit-cost analysis has been used by the US Army Corps of Engineers early in the twentieth century to evaluate dam and canals projects (Zerbe et al., 2010). This infrastructure has been of fundamental importance because it requires significant allocations of Government's budget (Zerbe et al., 2010). Prior to the US Army Corps, the French Government developed this tool to analyze public investments (Hanly and Spash, 1993). Later, it was an economist named Vilfredo Pareto in 1930, who settled the standards for BCA in the economic field through his work on income distribution and economic efficiency published much earlier in 1896. Then, in 1939 Nicholas Kaldor revised the concept of efficiency to a broader approach so that the Pareto criterion could be satisfied (Kaldor, 1939). This newly approach allowed projects were economic gains exceed economic losses fits the Pareto criterion (Zerbe et al, 2010).

In this study, we used a benefit cost ratio to set a comparison between potential tsunami losses and San Vicente resettlement costs. According to Randall (1987), any project which a ratio $B/C \geq 1.0$ is considered acceptable. The benefit cost ratio is expressed as follows:

$$\frac{B}{C} = \frac{\sum_{t=0}^T \frac{b_t}{(1+r)^t}}{\sum_{t=0}^T \frac{c_t}{(1+r)^t}} \quad (1)$$

where, b_t are benefits of the project over time, c_t are the cost over time, r is the discount rate, and t is the time period. In this study, benefits are denoted by bypassed cost of potential tsunami effects on San Vicente infrastructure, commerce, and human life through potential householders' income loss. Costs measure the resettlement cost of the entire community of San Vicente, which includes land acquisition costs.

We estimated benefits or avoided costs from the potential losses in land production which includes agricultural, livestock, fishing and aquaculture profit losses if a tsunami takes place, and it would take three years to have a full recovery from devastation, three years seems reasonable because recovering from tsunami effects it would require recuperate soil, acquiring new seeds and/or animals, planting, thinning and pruning, feeding animals, and wait to harvesting time. Additionally, fishing equipment such as boats, canoes and bongos potential losses were included and we counted as capital losses.

Tourism sector was also included in potential losses, and it was estimated from annual profits from several tourism activities in the area such as traditional sea food sales, hotel reservations, handcrafts sales, and so on. This information was recovered from the Territorial Development Strategic Plan of San Vicente parish (GAD San Vicente, 2011; GAD Canoa, 2011). Infrastructure potential losses were measured from local and national investment on infrastructure such as a highway passing by San Vicente, San Vicente's jetty, and a recreational park (MTOP, 2012).

Housing and property losses were estimated by means of two practical approaches due to the lack of real cadastral information in the municipality of San Vicente. One approach was estimated through the established percentages contained in the urbanism code of Galicia, Spain (Código de Urbanismo de Galicia, 2015) that explains the proportional relation of land use areas and the minimum spaces considered for constructions in a sustainable space when organizing the land of a community. These spaces on and under the land surface are associated to residential, industrial, commercial, hotel, green and community areas, as well as basic public services and communications. The construction costs for urbanization in Granada, Spain (Colegio Oficial de Arquitectos de Granada, 2012) were considered to estimate the losses in US dollars. This first approach makes use of the measured areas calculated in the San Vicente's cartography, the estimation of constructed and non-constructed areas using visual analysis on orthophotos, the cost of the square meter of construction provided by a five type classification (Dávila, 2015) corrected using interpolated values from the analysis and evolution of the main components costs of construction (Alemán et al., 2012) prepared by the Escuela Superior Politécnica del Litoral (ESPOL) Ecuador using the formula:

$$Cf = 1/n \cdot cctn \cdot cce \quad (2)$$

where Cf is the correction factor for cost of construction (m²), cct is the cost of construction (m²) by type of construction, cce is the cost of construction (m²) provided by the ESPOL study and n is the number of lots. Finally, the cost of loss per lot was calculated by the following expression:

$$Ctl = cct \cdot a \cdot (pcl + ptl) \cdot Cf \quad (3)$$

where Ctl is the total cost of a lot, cct is the cost of construction (m²) by type of construction, a is the area of the lot, plc is the percentage of area constructed in a lot, ptl is the percentage of land area in a lot and Cf is the correction factor.

The second approach considers the variable population (INEC, 2010) of San Vicente due to the urbanism code of Galicia uses the number of residential buildings and population distribution to calculate the different percentages of the different land use areas as well as utilities, services and common places for a new urbanization. The number of housing units needed was calculated as a ratio of 4 people per family, each family with a department of 70 m² and two departments per building (residential area). The population is 31.904 inhabitants and the residential area 279.160 m². Potential lost earnings as a result of a tsunami was measured based on the human capital approach to measure loss used in the United States instead of the willing to pay approach because we did not measure the value of life, which the latest approach is more appropriate (King and Smith, 1988). There are several conceptual models to estimate earning losses, but the human capital approach is the most widely used. In addition, we modified the model because we did not have the age when death occurred; neither had we differentiated between genders. We also did not consider not market losses, personal consumption offset, taxes (Government losses) and work life discounts. We simply took in account life expectancy (*E*), annual income (Income per capita for Ecuador (*Ii*), and the number of householder's death (*di*). Based on these information constraints, an equation to measure Potential Income lost (*Rp*) can be defined as follows:

$$Rp = i = 1/n \cdot E \cdot di \quad (4)$$

Annual income earnings I_i were discounted using the Banco Central of Ecuador borrowing rate, which is 0,0498, in addition we adjusted I_i to Ecuadorian inflation rate of 0,0353.

Resettlement cost included (RC) two major components, land acquisition (L) and housing, public services and infrastructure cost for a new community (C_n). Land acquisition was very straightforward estimation, price of land at the area (average price paid in historical land transactions in the area) and land's area, which was estimated using SIG tools ($L = p \times Q$). Resettlement cost of the new community (C_n) was more difficult since we had to include values for each public services, housing for householder, public buildings, open spaces, schools, hospitals, communication networks, commercial buildings and, so on. There are no known information regarding towns' planning and development from Ecuador, therefore we used instead guidelines and regulations from Communities of Granada and Galicia (Spain) for urban land and use planning. This happened because these communities share similar vision of how to display the man-land relationship with towns in Ecuador. These guidelines and regulations relate people with building area and these with minimum required space that it should take in account to build a sustainable space. Resettlement cost can be defined as:

$$RC = i = 1nL, C_n \quad (5)$$

4. RESULTS AND DISCUSSION

This study assumes that a tsunami would affect San Vicente town, having a probability of occurrence of 87 % being relatively high. Yet, if this natural hazard occurs it would have enormous effect not only in San Vicente, but in the country as well. We calculated and evaluated four different scenarios to estimate economic losses based on probable householders' death toll. In every scenario losses are significant as Table 1 indicates, the first scenario reaches almost 621 million US\$ and goes down to 441 million US\$ in the fourth scenario. Each scenario represents the avoided economic cost when compares to the resettlement cost. The analysis did not take in account several cost such as market losses, commerce, personal consumption offset, local such as property taxes and government taxes such as income, value-added tax, neither income increases throughout time, and work life discounts. Thus, these estimates could be much higher.

Table 1: Estimated economic losses if a tsunami hits the city of San Vicente, assuming 90% (Scenario 1), 80% (Scenario 2), 70% (scenario 3) and 50% (scenario 4) of death toll of San Vicente householders.

	SCENARIO 1 ¹	SCENARIO 2 ²	SCENARIO 3 ³	SCENARIO 4 ⁴
EARNINGS LOSSES	275,988,937.54	245,323,500.03	214,658,062.53	96,117,845.44
LAND LOSSES	22,549,178.49	22,549,178.49	22,549,178.49	22,549,178.49
PROPERTY LOSSES	303,928,877.94	303,928,877.94	303,928,877.94	303,928,877.94
INFRASTRUCTURE	11,508,905.74	11,508,905.74	11,508,905.74	11,508,905.74
CAPITAL/EQUIPMENT	358,353.83	358,353.83	358,353.83	358,353.83
TOURISM LOSSES	6,631,176.42	6,631,176.42	6,631,176.42	6,631,176.42
TOTAL 90%	620,965,429.96	590,299,992.46	559,634,554.95	441,094,337.87

The analysis shows that earnings and property losses are the most important values for each scenario. Potential earnings and property losses combined reach an average of 512 million US\$ of all scenarios, which is 92% of the total cost. As it was expected, earning losses would reduce in each scenario and its participation in total lost declines due to it is the only variable which really changes. Earning losses in scenario 1 is 44% of total economic losses and it is only 22% in scenario 4.

Current analysis did not consider recovery and reconstruction cost. In this kind of natural disaster, experiences from other cities around the world can show that it would take several weeks to fill basic needs such as food and water up to several years such us infrastructure and business. Then, in a different phase of this study, these costs should be evaluated as well.

Regarding the resettlement cost, land acquisition reached 1,8 million US\$, this value is based on land extension area of 357,61 ha including 26,25 linear park which runs along zone riverside (Fig. 4) multiply by 5.170,17 US\$/ha which is the average price in local land transactions.

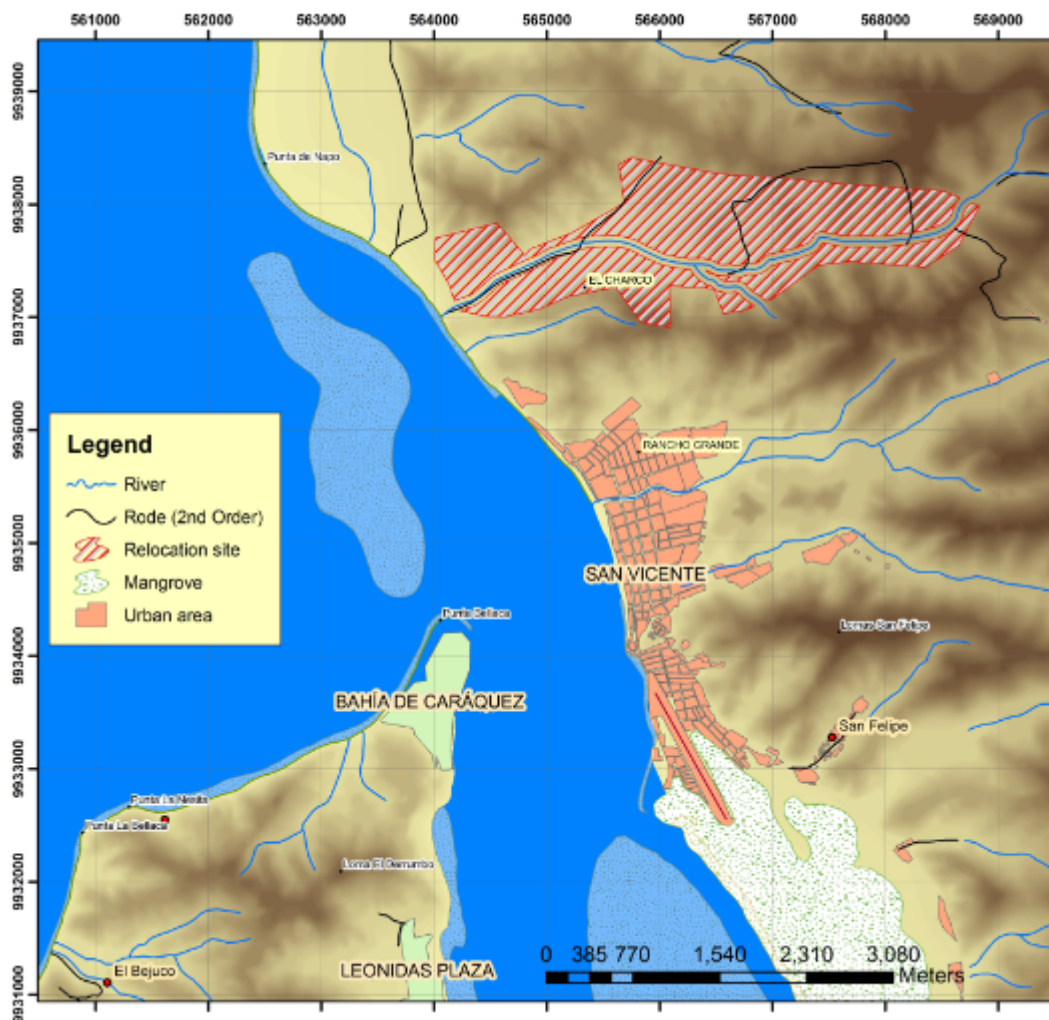


Figure 4: Relocation site to be built for “new” San Vicente

The resettlement cost for a new city (*C_n*) reached 374,4 million US\$. This value includes residential cost, open and public spaces, recreational parks, school buildings, communication network, commercial buildings, social gears, hotel areas, industrial area, churches, hospitals, other social and public services, and open community spaces. The summary of the resettlement costs detailed in Table 2 and provide a total cost for reconstruction being approximately \$ 374'433,189.46 US\$.

Table 2: Construction costs

Concept	Costs based on estimated areas
1 SUPPLY NETWORK AND BASIC SERVICES	119.417.676,79
2 RESIDENTIAL AREA	86.928.245,16
3 OPEN SPACES OF PARKS AND GREEN AREAS	57.723.614,60
4 EDUCATIONAL INFRASTRUCTURE	38.865.171,25
5 COMMUNICATIONS NETWORK	15.212.442,90
6 COMMERCIAL EQUIPMENT	15.212.442,90
7 SOCIAL EQUIPMENT	15.212.442,90
8 HOTEL AREA	15.212.442,90
9 INDUSTRIAL AREA	3.042.488,58
10 PUBLIC AND SOCIAL INTEREST SERVICES	3.803.110,73
11 COMMUNITY PUBLIC SPACE	3.803.110,73
Total cost of reconstruction	374.433.189,46

We selected this first approach to evaluate if e resettlement is feasible because it provides more detail in different costs involved town reconstruction. Yet, with the second approach, we had an increase of 5% in resettlement value.

The special distribution of new buildings and other areas as a percentage of the total area is presented in figure 5. Complete resettlement cost reaches 376.28 million US\$. Yet, as in the case of the avoided cost, resettlement is a process that takes several months, even years. We limited our analysis to building a new town with all facilities, however resettlement means not only constructing a new town, it also means contacting beneficiaries, discussing alternatives, socializing towards get consensus in the population. All these transaction cost should be considered and would rise the resettlement cost.

The estimate resettlement cost is compared to previously establish avoided cost in order to establish the avoided cost-resettlement cost ratio. The ratio indicates that if a project such as what we are proposing here is valuable in the economic sense. Therefore, the ratio implies that each scenario has a higher value than any resettlement cost (Table 3), meaning that in terms of human life, housing, and infrastructure and business relocation of San Vicente should be considered by authorities and policy makers.

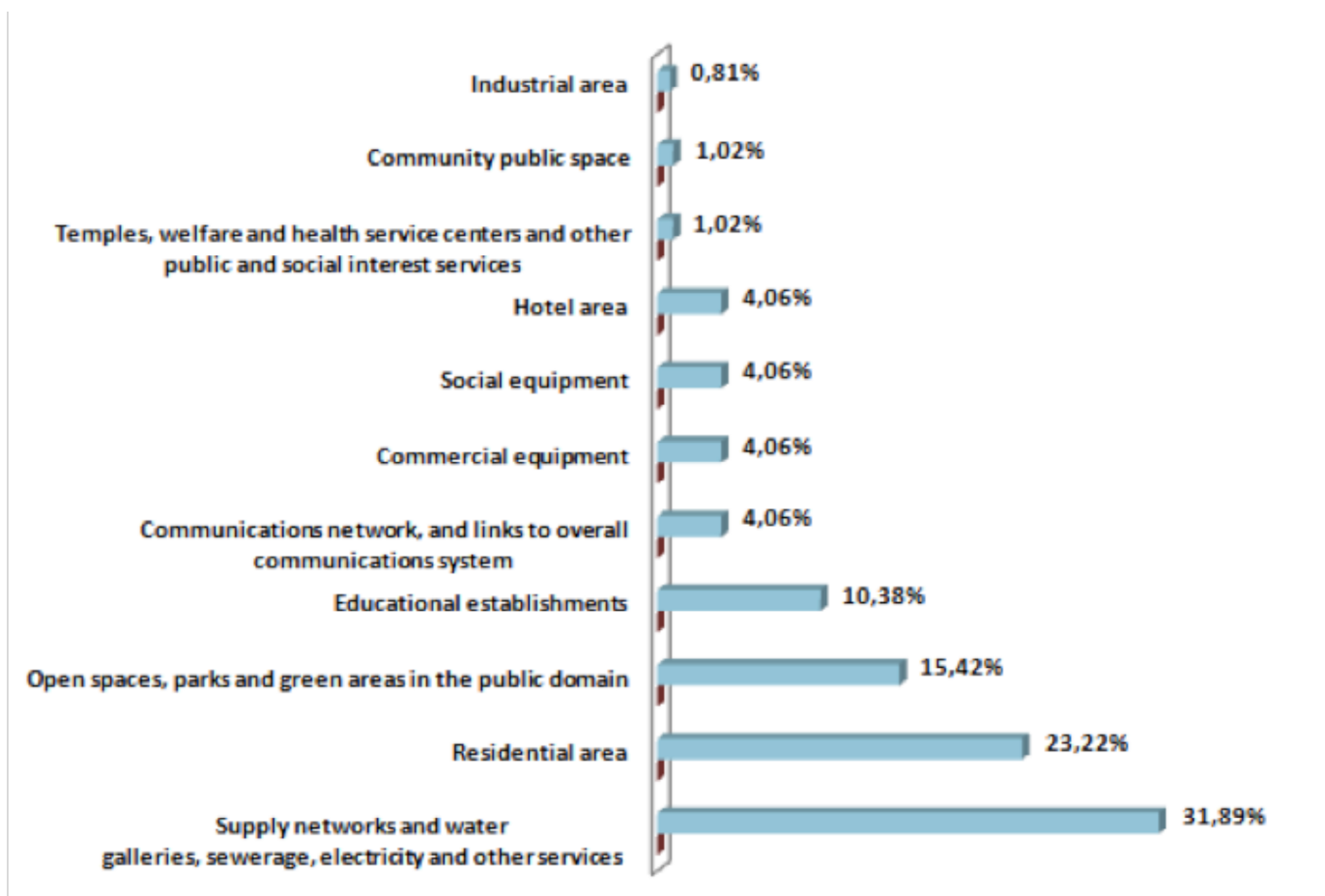


Figure 5: Percentage and relation of areas to be built for a “new” San Vicente

Table 3: Avoided/Resettlement Cost Ratio

	AVOIDED COSTS, DIFFERENT SCENARIOS				RESETTLEMENT COSTS
	1	2	3	4	
ECONOMIC COSTS	620.965.430	590.299.992	559.634.555	441.094.338	376.282.083
RATIO B/C	1,65	1,57	1,49	1,17	1,00

5. CONCLUSION

Resettlement usually occurs after a disaster strikes, but in terms of human life, this should not be the case for the regular public policy. That results, that in this study for the town of San Vicente in western Manabi Province, we were able to present how using well-known evaluation tools such as BCA, SIG and other analysis tools can help policy makers to prevent future disastrous results by all means in order to accomplish an intelligent prevention and reduction of vulnerabilities and losses of life.

ACKNOWLEDGMENTS

We are indebted to the citizens of San Vicente for their generous support during fieldwork and to the municipality of San Vicente providing useful data for our study. We also thank the Universidad de las Fuerzas Armadas ESPE for logistic and financial support.

REFERENCES

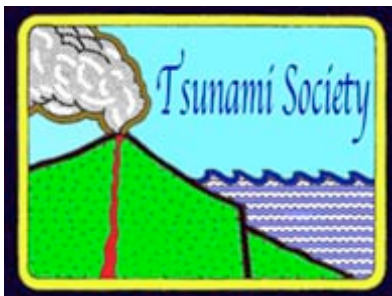
- Alemán F., Vera, J. and Ordeñana, X., 2012: Análisis y evolución de los costos de los principales insumos del sector de la construcción en el Ecuador en el período 2004-2011. Guayaquil, ESPOL, Ecuador: 133pp
- Aon Benfield, 2015: 2014 Annual Global Climate and Catastrophe Report, Impact Forecasting. Aon Benfield Risk, Reinsurance and Human Resources. Aon plc. (http://thoughtleadership.aonbenfield.com/Documents/20150113_ab_if_annual_climate_catastrophe_report.pdf)
- Athukorala, P. and B. Resosudarmo. 2005: The Indian Ocean Tsunami: economic impact, disaster management, and lessons. Division of economic Research School of Pacific and Asian Studies, Australian National University, Canberra Australia.
- Athukorala, P. C. and Resosudarmo, B. P., 2005: The Indian Ocean Tsunami: economic impact, disaster management, and lessons. *Asian Economic Papers*, 4, (1): 1-39.
- Barcená, A., A. Prado, L. López and J.L. Samaniego. 2010. The Chilean earthquake of 27 of February 2010: an overview. Disaster Assessment Unit of ECLAC, United Nations Publications, Santiago, Chile.
- Beck, S.L. and Ruff, L.J., 1984: The rupture process of the great 1979 Colombia earth-quake: evidence for the asperity model. *J.Geophys. Res.*89: 9281–9291
- Bianucci, G., Cantalamessa, G., Landini, W., Ragaini, L., Valleri, G., 1997. Paleontological and sedimentological observations on the Canoa Formation. *Bollettino della Società Paleontologica Italiana* 36, 85–96.
- Chunga, K. and Toulkeridis, T. (2014). First evidence of paleo-tsunami deposits of a major historic event in Ecuador. *J. Tsunami Soc. Int*, 33: 55-69.
- Código de Urbanismo de Galicia, 2015: Agencia Estatal Boletín Oficial del Estado, Spain: 312pp
- Colegio Oficial de Arquitectos de Granada, 2012: Costes de referencia de la construcción. Granada, Spain: 5pp
- Cruz D' Howitt, M. and N.E. Vásquez.2010. Elaboración de 33 cartas – croquis de amenazas por tsunami y análisis de riesgos en la costa ecuatoriana utilizando indicadores geomorfológicos y socioambientales. *Revista Geoespacial* No 7: 1-20.
- Cruz D'Howitt, M., Acosta, M.C. and Vásquez. N.E., 2010. Riesgo por Tsunami en la Costa Ecuatoriana. Instituto Panamericano de Geografía e Historia, Sección Nacional del Ecuador , Organización de los Estados Americanos – OEA. Publicaciones: 15pp.
- Daniell, J.E., F. Wenzel, and B. Khazai. 2010. The Cost of Historical Earthquakes Today – Economic Analysis since 1900 through the use of CATDAT. Paper presented at the Australian Earthquake Engineering Society 2010 Conference, Perth, Western Australia: 15 pp.

- Egbue, O. and Kellogg, J., 2010: Pleistocene to Present North Andean “escape”. *Tectonophysics* 489: 248-257.
- English, R., and F.E. Brusberg. 2002. Handbook for Preparing a Resettlement Action Plan. International Finance Corporation, Environmental and Social Development Department. Washington DC. 93 pp.
- González-Riancho, P., B. Aliaga, S. Hettiarachchi, M. González, and R. Medina. 2015. A contribution to the selection of tsunami human vulnerability indicators: conclusions from tsunami impacts in Sri Lanka and Tahiland (2004), Samoa (2009), Chile (2010) and Japan (2011). *Natural Hazards and Earth System Science* 15: 1493-1514.
- Gusiakov, V.K., 2005: Tsunami generation potential of different tsunamigenic regions in the Pacific. *Marine Geology*, 215, 1-2: 3-9.
- Gutscher, M.A., Malavieille, J.S.L. and Collot, J.-Y., 1999: Tectonic segmentation of the North Andean margin: impact of the Carnegie ridge collision. *Earth Planet. Sci. Lett.* 168: 255–270.
- Hanley, N. and C.L. Spash. 1993. Cost-benefit Analysis and the Environment. Aldershot, Hants, England: E. Elgar Publishers. 275pp
- Harpp, K. S. and White, W. M. (2001). Tracing a mantle plume: Isotopic and trace element variations of Galápagos seamounts. *Geochemistry, Geophysics, Geosystems*, 2(6).
- Harpp, K. S., Fornari, D. J., Geist, D. J. and Kurz, M. D. (2003). Genovesa Submarine Ridge: A manifestation of plume-ridge interaction in the northern Galápagos Islands. *Geochemistry, Geophysics, Geosystems*, 4(9).
- Holden, J. C. and Dietz, R. S. (1972). Galapagos gore, NazCoPac triple junction and Carnegie/Cocos ridges. *Nature*, 235, 266-269.
- INEC. (2010). Censo Nacional de Población y Vivienda. Quito: Instituto Ecuatoriano de Estadística y Censos.
- Ioualalen, M., Ratzov, G., Collot, J. Y. and Sanclemente, E. (2011). The tsunami signature on a submerged promontory: the case study of the Atacames Promontory, Ecuador. *Geophysical Journal International*, 184(2), 680-688.
- Jayatilleke, B. and A. Naranpanawa. 2007. The economic effects of the Asian tsunami on the tear drop in the Indian Ocean: a general equilibrium analysis. *South Asia Economic Journal*, 8(1): 65-85.
- Kaldor, N. 1939. Welfare propositions of economics and interpersonal comparisons of utility. *Economic Journal* 49 (195): 549-552.
- Kanamori, H. and McNally, K.C., 1982: Variable rupture mode of the subduction zone along the Ecuador–Colombia coast. *Bull. Seismol. Soc. Am.* 72 (4): 1241–1253.
- Kelleher, J.A., 1972: Ruptures zones of large South American earthquakes and some predictions. *Journal of Geophysical Research*, 77, 11: 2087-2103.
- Kellogg, J.N. and Vega, V., 1995: Tectonic development of Panama, Costa Rica and the Colombian Andes: Constraints from Global Positioning System geodetic studies and gravity. *Geol. Soc. Am. Special Paper* 295, 75–90.
- King, E.M. and J.P Smith. 1988. Computing Economic Loss in Cases of Wrongful Death. RAND Publication Series, The Institute for Civil Justice. The RAND Corporation, Santa Monica CA. 160 pp.
- Ministerio de Transporte y Obras Públicas - MTOP. 2012. Obras que generan cambio: San Vicente se une al desarrollo vial. Dirección de Comunicación Social y Atención al Ciudadano, Ministerio de Transporte y Obras Públicas. 7 pp.

- National Police Agency of Japan. 2015. Damage Situation and Police Countermeasures associated with 2011 Tohoku district - off the Pacific Ocean Earthquake. National Police Agency of Japan, Emergency Disaster Countermeasures Headquarters. (http://www.npa.go.jp/archive/keibi/biki/higaijokyo_e.pdf)
- NOAA/Pacific Tsunami Warning Center. 2015. Amplitudes for the 16 September 2015 Central Chile tsunami. Obtained from Pacific Tsunami Warning Center (PTWC). Tsunami Bulletin Board, Pacific Tsunami Warning Center. (http://www.ngdc.noaa.gov/nndc/struts/results?EQ_0=5590&t=101650&s=9&d=100,91,95,93&nd=display)
- Pararas-Carayannis, G. 1980: The Earthquake and Tsunami of December 12, 1979, in Colombia. Intern. Tsunami Information Center Report, Abstracted article in Tsunami Newsletter, Vol. XIII, No. 1.
- Pararas-Carayannis, G., 2012: Potential of tsunami generation along the Colombia/Ecuador subduction margin and the Dolores-Guayaquil Mega-Thrust. *Science of Tsunami Hazards*, 31, 3: 209-230.
- Pareto, V. 1896. *Cours d'économie politique professé à l'Université de Lausanne*. Lausanne: F. Rouge. 426pp
- Pilger, R. H. (1983). Kinematics of the South American subduction zone from global plate reconstructions. *Geodynamics of the eastern Pacific region, Caribbean and Scotia arcs*: 113-125.
- Pontoise, B. and Monfret, T. (2004). Shallow seismogenic zone detected from an offshore–onshore temporary seismic network in the Esmeraldas area (northern Ecuador). *Geochemistry, Geophysics, Geosystems*, 5(2).
- Randall, A. 1987/ *Resource Economics: An Economic Approach to Natural Resource and Environmental Policy*. John Wiley & Son, Inc. Publishers. New York: 247-250.
- Raschky, P.A. 2008. Institutions and the losses from natural disasters. *Natural Hazards and Earth System Science* 8: 627-634.
- Ratzov, G., Collot, J. Y., Sosson, M. and Migeon, S. (2010). Mass-transport deposits in the northern Ecuador subduction trench: Result of frontal erosion over multiple seismic cycles. *Earth and Planetary Science Letters*, 296(1), 89-102.
- Ratzov, G., Sosson, M., Collot, J. Y., Migeon, S., Michaud, F., Lopez, E. and Le Gonidec, Y. (2007). Submarine landslides along the North Ecuador–South Colombia convergent margin: possible tectonic control. In *Submarine Mass Movements and Their Consequences*. Springer Netherlands: 47-55
- Reynaud, C., Jaillard, É., Lapierre, H., Mamberti, M. and Mascle, G. H. (1999). Oceanic plateau and island arcs of southwestern Ecuador: their place in the geodynamic evolution of northwestern South America. *Tectonophysics*, 307(3): 235-254.
- Rudolph E. and Szirtes S., 1911: Das kolumbianische Erdbeben am 31 Januar 1906, *Gerlands Beitr. z. Geophysik*, 2: 132- 275.
- Shepperd, G.L. and Moberly, R., 1981: Coastal structure of the continental margin, northwest Peru and southwest Ecuador. *Geological Society of America Memoirs*, 154: 351-392,
- Swenson, J.L. and Beck, S.L., 1996: Historical 1942 Ecuador and 1942 Peru subduction earthquakes, and earthquake cycles along Colombia–Ecuador and Peru subduction segments. *Pure Appl. Geophys.* 146 (1): 67–101.

- The World Bank, 2004: Involuntary Resettlement Sourcebook: Planning and Implementation in Development Projects. The International Bank for Reconstruction and Development – The World Bank. Washington DC: 472 pp.
- Toulkeridis, 2011: Volcanic Galápagos Volcánico. Ediecuatorial, Quito, Ecuador: 364 pp
- Toulkeridis, T., 2013: Volcanes Activos Ecuador. Santa Rita, Quito, Ecuador: 152 pp
- United States Geological Service (USGS), 2015: Historic Earthquakes, 1906 January 31st. (http://earthquake.usgs.gov/earthquakes/world/events/1906_01_31.php)
- Zerbe, R.O Jr, T.B. Davis, N. Garland, and T. Scott. 2010. Toward Principles and Standards in the Use of Benefit-Cost Analysis. Benefit Cost Analysis Center, University of Washington. Seattle WA. 115 pp.

ISSN 8755-6839



SCIENCE OF TSUNAMI HAZARDS

Journal of Tsunami Society International

Volume 35

Number 1

2016

Copyright © 2016 - TSUNAMI SOCIETY INTERNATIONAL

TSUNAMI SOCIETY INTERNATIONAL, 1741 Ala Moana Blvd. #70, Honolulu, HI 96815, USA.

WWW.TSUNAMISOCIETY.ORG